Detecting Alzheimer's Disease based on Structural Region Analysis using a 3D Shape Descriptor

Kauê T N Duarte*, David G Gobbi†, Richard Frayne† and, Marco A G de Carvalho*
*School of Technology, University of Campinas, 13484-332 - Limeira, SP, Brazil
Email: kaue.unicamp2011@gmail.com, magic@ft.unicamp.br
†Calgary Image Processing and Analysis Centre, Departments of Radiology and Clinical Neurosciences,
Hotchkiss Brain Institute, University of Calgary, Calgary, AB, Canada T2N 2T9
Email: dgobbi@ucalgary.ca, rfrayne@ucalgary.ca

***Abstract*—Alzheimer's disease (AD) is a common neurodegenerative dementia that affects older people. Changes in behavior and cognition are the most common characteristics of this disease and are associated with changes in brain structure. Techniques focusing on brain shape have been recently proposed to quantify and understand these changes. One challenge when examining AD is that each anatomical region may have a unique role in and time course for brain deterioration, requiring a whole-brain method that is capable of individual (or regional) analyses at different disease stages. We propose to apply the scale-invariant heat kernel signature descriptor to magnetic resonance brain images in order to evaluate regional shape features across different brain regions. We measured the shape feature similarity in 500 subjects, equally divided across five progressive, disease-based stages. The shape analysis provided a complementary perspective to whole-brain analysis, due to the capability of identifying how different structures degenerate at different rates in the brain. In total, a group of 99 distinct brain regions belonging to cortical and deep gray matter were analyzed across the five disease stages. Preliminary assessment of shape-based analysis of key brain regions demonstrated that SIHKS was predictive of disease stage and disease progression.**

I. Introduction

Alzheimer's disease (AD) is a neurodegenerative dementia that affects about half of the global population (>85 years). This disease compromises both brain structure and function, leading to deleterious affects on behavior and cognition. Mild cognitive impairment (MCI) is proposed as an intermediate (or prodromal) stage of AD. Even in the absence of a proven treatment for AD, accurately predicting early signs of AD is important, for it may improve patient management and allow appropriate use of emerging disease-modifying therapies. The Alzheimer's Disease Neuroimaging Initiative (ADNI) divided progression into five disease stages, ranging from normal control (CN), early MCI (eMCI), MCI, late MCI (lMCI), to AD.

Previous imaging studies have demonstrated that the shape of brain structures is altered with AD progression. For example, a number of brain structures consistently shrink in neurodegeneration. Hippocampal volume loss, as one example, can begin early in AD patients and typically ranges from -4% to -6% volume change per year [1]. Other brain structures have differing onset times and rates of changes. The rate of regional change may vary across the different AD stages. Fig. 1 illustrates the shape of some brain structures in representative CN and AD subjects.

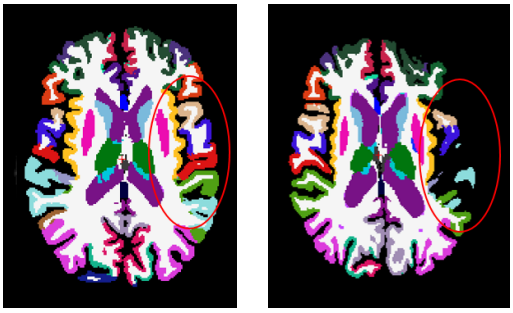

(a) **(b)**

Fig. 1. Segmented T1-weighted magnetic resonance (MR) images (using Freesurfer) for (a) CN and (b) AD subjects. The red circle on the right side of each image highlights changes in shape and reductions in volume for gray and white matter (as expected in AD). AD = Alzheimer's disease, CN = normal control.

One analysis approach is to apply feature-based techniques to create a bag-of-features and then use these results either with conventional image processing or, more recently, machine learning approaches. There are many different types of descriptors that target specific features including color, texture and, the focus of this work, shape.

Brain imaging is used to aid the assessment of AD by identifying regional anatomical brain changes and correlating them to the five AD stages. Imaging is a common examination for understanding brain disease. The efficacy of combining different examinations has been previously highlighted. Our focus was to develop a method capable of identifying shape variations and to differentiate the stages of AD progression.

In this paper, we present a method based on estimating the similarity among AD-related stages by applying shape description techniques to each anatomical brain region. These estimates use the scale-invariant heat kernel signature (SIHKS), clustering geometric words using k-means, and similarity measurements based on covariance.

The main contributions of this work can be summarized as follows: 1) Implementation of a 3D-mesh scale-invariant shape descriptor for brain region description; and 2) Testing of an

approach for classification based on shape feature extraction, clustering, and similarity measurements.

The remainder of this work is organized in the following sections: In Section II we summarize related work. The proposed method and details of each step is addressed in Section III. Section IV presents and interprets the results and Section V discusses our findings. We summarize this work and present our conclusions in Section VI.

II. Related Work

Shape analysis has a variety of applications in image processing. Liu *et al.* [2] proposed a slice-by-slice putamen segmentation method that combines wavelets and a neural network. Their approach was to: 1) crop a proton density-weighted MR image (including the putamen), and extract the features using 1D wavelet decomposition; 2) classify the putamen and find its location using a neural network; 3) segment the object with contrast-limited adaptive histogram equalization. The image was then classified into two clusters using fuzzy C-means; and 4) finally, the classification of putamen shape was performed using a neural network using features extracted within the putamen region of interest. Their work highlighted that shapes can be described by their moments and they demonstrated accurate detection of the putamen shape.

Jia-Lin *et al.* [3] introduced a region growing algorithm for computerized tomography (CT) images that considers shape features. They proposed a chart-transferring tree that took into account different adjacent regions in the brain. Their method considered shape roundness based on perimeter and normalized moment of inertia. They demonstrated their method by identifying normal and abnormal cerebral hemorrhage images and obtained an accuracy of 88.3%.

Zhu *et al.* [4] presented a method to distinguish subjects based on their brain shape differences. Their approach relies on an optimal hierarchical feature matching approach. They used spatial pyramid matching, which was divided into four steps: 1) *Image Preprocessing*, carrying out edge preservation filtering; 2) *Feature Extraction* based on Canny edge detection; 3) *Feature Labelling* using definitions from a codebook; and 4) *Evaluation* of image pairs based on multilevel feature histograms. For feature labelling, they captured the anatomical shape and then used SPM [5] to perform matching using a set of feature maps. Their key idea was to avoid mismatching along near edges. Each edge was clustered using k-means and some artifacts are removed using fuzzy-C-means.

Addressing the difficult task of detecting brain tumors based on their irregular shape, Ghanavati *et al.* [6] proposed a multi-modality framework for tumor detection. They used MR images as input due to their structural characteristics. Their framework had two key phases: 1) *Training*: MR images (*e.g.*, T1, T2, gadolinium contrast enhanced) were pre-processed to reduce the intensity bias and remove non-brain tissue. They subsequently extracted signal intensity, symmetry, shape, and texture features from these images. Shape features were extracted using 3D non-rigid Demons registration. They then used these features in AdaBoost to select the most discriminative features and thus generated a set of selected and trained features. 2) *Detection*: Images were preprocessed using the same workflow as in the training phase. Selected features were used for feature extraction. After classification, the trained features were used to segment the tumor.

They developed a multi-modal framework capable of reaching an accuracy of nearly 90%, demonstrating that shape features can improve segmentation procedures.

Chaddad *et al.* [7] highlighted the importance of identifying how the brain is affected in AD by analyzing distinct regions. Their analysis used 235 individuals selected from the OASIS dataset [8] and took into account texture and shape changes in CN subjects and AD patients using a four-stepped approach: 1) *Segmentation*: Using Freesurfer [9], they obtained a segmentation of the brain that labeled 41 subcortical regions of interest; 2) *Feature Extraction*: Radiomic features of heterogeneity and shape of subcortical regions were extracted. Other features characterizing properties, such as contrast, texture strength and complexity were also extracted. Combining all extracted features, they obtained a 35-element texture-feature vector. In addition, they extracted four shape features to characterize the surface of each region; and 3) *Analysis and Classification*: A five-layer 3D convolutional neural network (CNN) was applied to classify these features and produce 21 distinct feature maps. Wilcoxon tests were applied to identify significant differences in subcortical brain regions. The authors found that the two regions (the hippocampus and amygdala) had significant differences between CN and AD patients.

Rajendran and Madheswaran [10] proposed a system to combine low-level features (images) and high-level knowledge (specialists). They used CT images as input in order to identify benign and malignant tissue. Their system had four steps: 1) *Training*, which performs the histogram equalization, segmentation using curve evolution and shape correction, feature extraction, and feature vectors; 2) *Testing*, which performs the same procedures described in the training phase but on the test data; 3) *Mining*, which uses a transactional database (obtained in the first step) to perform association rule mining (obtained in the second step) and to generate a set of association rules; and 4) *Classification*, which applies these rules to classify whether a subject is normal or abnormal. In case of abnormality, they are further classified as benign or malignant subjects. Their results showed 97% sensitivity, 91% specificity, and 98.5% accuracy. They concluded this approach can support physicians for classification of malignant tissue.

Shape features in image analysis have been well studied in the literature. Bu *et al.* [11], for example, proposed a multi-level 3D shape feature extraction approach for image retrieval tasks. Their approach sequentially combined shape feature extraction and deep learning in order to classify general shapes. This four-step approach is composed of: 1) *Low-level Feature Extraction*: HKS [12], SIHKS [13] and average geodesic distance were calculated in order to convert each shape into a representative shape feature matrix. 2) *Mid-level Features*: bag-of-features were computed in order to represent

features as geometric words, with the generation of geometric words are obtained by using k-means. 3) *High-level Features*: firstly, a restricted Boltzmann machine (RBM) is applied to learn the middle-level features, and secondly, those RBM are stacked and learned using a deep belief network (DBN). They calculated an accuracy of 70% for twenty types of shapes, they also highlighted the need of using more data to improve the fitting during the training phase.

Zhou *et al.* [14] suggested another approach that performs segmentation using shape information. In order to capture shape information, they used a shape-learning network that incorporates affine-invariant transformations. Their approach included: 1) *Shape Learning*: where the shape information is compared and affine pair examinations from a subject are trained, thus making the approach shape-aware; and 2) *Shape-guided Segmentation*: Training of the segmentation network in order to generate the segmentation label map. The authors examined the left and right hippocampus and caudate, and used Dice and Hausdorff distance metrics to show that the proposed approach performed accurate segmentation.

Our work differs from these summarized approaches in that:

1) We aim to identify distinct region changes over the full range of AD progression, and not only in late stages;
2) We developed software to aid the identification of the best image for each patient, thus possibly reducing the influence of artifacts; and
3) We applied the SIHKS algorithm [13] in the context for 3D shape description of region meshes.

III. Proposed Method

Our method consists of four major steps:

1) *Data Acquisition and Selection*: Obtaining data and selecting the best examination per patient;
2) *Brain Segmentation and Meshing Conversion*: Using Freesurfer segmentation of the brain into regions [9] and conversion of each region into a mesh;
3) *Feature Extraction*: Applying SIHKS [13] to the meshes and extracting shape information (*i.e.*, heat diffusion);
4) *Similarity Measurement*: Comparing the co-variance among patterns from specific regions.

The proposed analysis pipeline is illustrated in Fig. 2 and each step is discussed in detail in the following sub-sections.

A. Data Acquisition and Selection

Data Acquisition. Data used in the preparation of this article were obtained from the ADNI database (adni.loni.usc.edu). The ADNI was launched in 2003 as a public-private partnership, led by Principal Investigator Michael W. Weiner, MD. The primary goal of ADNI has been to test whether serial magnetic resonance imaging, positron emission tomography, other biological markers, and clinical and neuropsychological assessment can be combined to measure the progression of MCI and early AD. The following information was provided by the initiative: Image Data ID, Subject ID, AD Stage, *i.e.*, one of {CN, eMCI, MCI, lMCI, AD}, Sex, Age, Description, and Acquisition Date.

Two constraints were applied in the ADNI search query: 1) only T1-weighted (T1w) MR images were selected; and 2) the Description field had to include "*Rage*" or "*FSPGR*". The search query outcome retrieved $16,273$ entries (examinations) in $1,556$ subjects. There was an average of 10.5 ± 6.3 (mean $\pm$ standard deviation) examinations per subject.

The search results were next filtered by acquisition date, in order to retrieve the most recent examination per patient. Because the ADNI acquisition protocol repeated T1w scanning, many subjects had repeated examinations on the same day, this step identified $3,326$ examinations grouped over the $1,556$ subjects. After this step, there was an average of 2.1 ± 0.5 same-day examinations per subject.

Patient Volume Selection (PVS) Tool. In order to select the "best" of the same-day MR examinations per patient, we developed an interactive software program (Patient Volume Selection Tool) to allow visual selection of the images. The tool was a grid-interactive tool and designed to facilitate selection of the "best" image volume. The key idea behind this tool was to interactively facilitate selection of the image volume with the least amount of image artifact. Such artifacts can arise from voluntary and involuntary patient motion.

The tool interface is straightforward. consisting of a grid of entries. Each displayed column consists of one subject and each row contains different scans (Fig. 2.1). In some cases, a column might have just one selected cell; though per the ADNI acquisition protocol, most columns contained at least two cells. (The software is publicly available at [15]).

We selected a set of 500 T1-w MR volumes (100 for each of five disease stages: CN = normal control, eMCI = early mild cognitive impairment, MCI, lMCI = late MCI, and AD). The demographic information for the selected subjects is summarized in Table I.

B. Brain Segmentation and Mesh Conversion

Brain segmentation. Freesurfer was used to segment the brain [9], the pipeline can be grouped into the following three steps: 1) image normalization and skull stripping; 2) smoothing and inflation of the surface; and 3) registration and cortical parcellation. We used the DKT [16] parcellation provided by Freesurfer. We restricted the Freesurfer output to 99 gray matter regions. The assigned region ID is standardized, allowing structures in different subjects to be compared by region IDs. Each region was turned into binary volume, where voxel intensity was set to 1 inside the region and 0

TABLE I
Demographic information of the selected subjects.

Attribute	CN (N=100)	eMCI (N=100)	MCI (N=100)	lMCI (N=100)	AD (N=100)
Age (years)					
median	79	73	80	74	77
(range)	(61 to 95)	(56 to 87)	(55 to 92)	(57 to 93)	(57 to 89)
Gender					
% male	54%	47%	70%	50%	55%

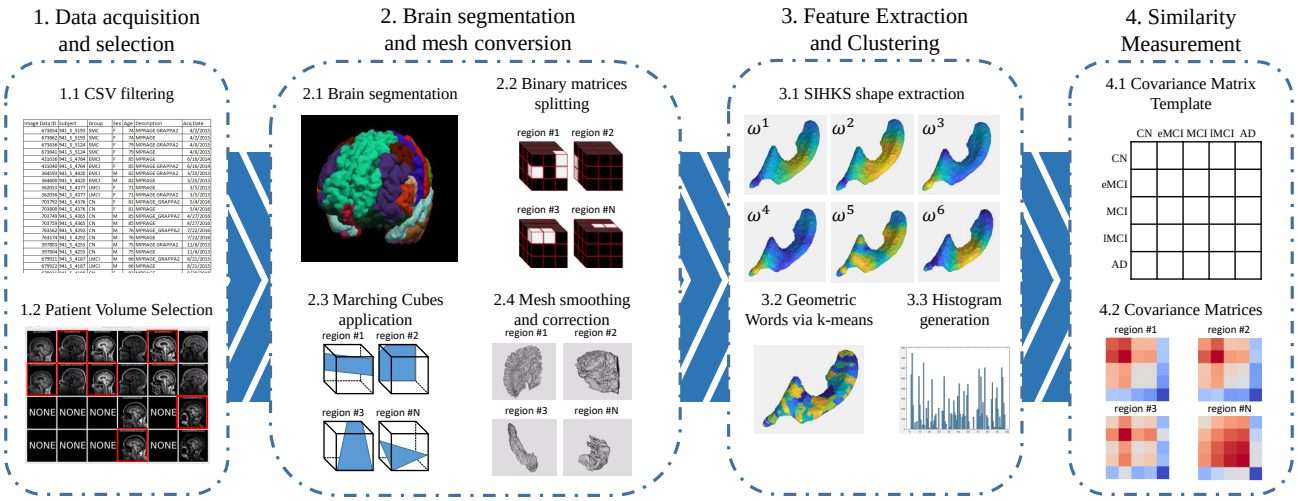

Fig. 2. Overview of the proposed method for shape feature extraction.

otherwise.

Mesh Conversion. To provide the input required by the shape descriptor, we generated meshes for each region. Meshes are structures that represent information as a set of points (nodes) and faces (surfaces defined by the connected points). We used the marching cubes algorithm [17] to convert regions to meshes. This algorithm extracts polygonal meshes from a three-dimensional volume.

Mesh conversion followed these steps: 1) The marching cubes algorithm was applied; 2) The resulting mesh was smoothed using a 3×3 Laplacian kernel; 3) The largest connected-component was selected (*i.e.,* the outer shape), thus avoiding small inner holes that may cause the feature identification to fail; and 4) As necessary, the face normal vectors were inverted so they faced outward with respect to the region.

C. Feature Extraction and Clustering

Feature Extraction. Assuming that regional shape varies with AD stage, we chose a shape descriptor that was sensitive to these changes. SIHKS is considered a robust local shape descriptor and insensitive to scale deformations. [13]

The related HKS is invariant to isometric deformation, but not invariant to scale. Given a manifold mesh X, its heat diffusion equation is defined as:

$$\left(\Delta + \frac{\partial}{\partial t}\right) u(x,t) = 0 \tag{1}$$

where Δ is the negative Laplace-Beltrami operator, and $u(x,t)$ is the heat distribution of a given point x at time t.

Sun *et al.* [18] adopted the main diagonal of the heat kernel as a feature descriptor. Each point x on the surface has a specific feature vector that represents its HKS, as calculated by:

$$\mathrm{HKS}(x) = c(x)(K_{t1}(x,x), ..., K_{tn}(x,x)) \tag{2}$$

where $c(x)$ satisfies $\|\mathrm{HKS}(x)\|_2 = 1$. Eq. 2 gives the quantity of heat at a given point x after a given time t. The calculation of HKS considers the first eigenvalues and eigenfunctions of the Laplace-Beltrami operator.

One drawback of HKS is that it is very sensitive to scaling. To suppress this limitation, Bronstein *et al.* [13] proposed the SIHKS, described in the following equations:

$$h_{\mathrm{diff}}(x) = (\log K_{\alpha^{\tau 2}}(x,x) - \log K_{\alpha^{\tau 1}}(x,x), \\ ..., \log K_{\alpha^{\tau m}}(x,x) - \log K_{\alpha^{\tau m-1}}(x,x)) \tag{3}$$

$$\mathrm{SIHKS}(x) = \left\| \left(F_{h_{\mathrm{diff}}}(x)\right)(\omega_1, ..., \omega_6) \right\| \tag{4}$$

where F is the discrete Fourier Transform, and ω is a given frequency.

Clustering. The next step was to generate the bag-of-features in order to represent the occurrences of geometric words. Geometric words are defined as transitions that occur in a specific shape. In order to generate a geometric vocabulary, we used the k-means technique, a clustering algorithm that automatically partitions data into a set of k clusters.

k-means is performed independently in each brain region. Thus, each region has a set of 500 meshes. The clustering procedure occurs in three steps:

1) For each region, we defined a matrix A of size $N \times M$, where N is equal to the number of patients multiplied by the number of mesh points belonging to that patient, and M is equal to the number of descriptors (*i.e.*, 6). This matrix is clustered using k-means, thus generating a matrix B($N \times 1$). In our experiments, we used $k = 100$, which provided robust convergence for the clustering.
2) The matrix B was inserted back into the original matrix, in order to return the same labeled point to the patients.
3) Each set of labeled points was then stored as a histogram. Thus, each patient has 99 histograms, one per region.

D. Similarity Measurement

The similarity measurement step regards the comparison among all subjects. The covariance (cov) is calculated using:

$$\text{cov}(x, y) = \frac{1}{n}\sum_{i=1}^{n}(x_i - x_j)(y_i - y_j) \quad (5)$$

A 500×500 matrix stored the similarity values for all subjects.

E. Evaluation Metrics

We adopted four metrics to evaluate our method: 1) Sensitivity (Se) also know as Recall (R), 2) Specificity (Sp), 3) F-score (F), and 4) Accuracy (Acc). These metrics were calculated from the false-positive (FP), true-positive (TP), false-negative (FN), and true-negative (TN) rates in the 2×2 confusion matrices. The evaluated metrics were obtained using:

$$Se = R = \frac{TP}{TP + FN}, \quad Sp = \frac{TN}{FP + TN},$$
$$F = 2 \times \frac{P * R}{P + R}, \quad \text{and } Acc = \frac{TP + TN}{TP + TN + FP + FN}.$$

where the precision is defined as $P = \frac{TP}{TP+FP}$.

F. Implementation

Our method was entirely implemented using the following freely-available packages:

1) Demographic data was processed using Python 2.7 Jupyter Notebook. Our Patient Volume Selection software was developed in Python 2.7 using PyQt;
2) Segmentation of the brain used Freesurfer [9]. The binary volumes were obtained using Python 2.7, and the marching cubes algorithm and mesh smoothing and correction were implemented using VTK;
3) The feature shape extraction and the clustering were implemented in Matlab (version r2018a) using the Image Processing Toolbox; and
4) The similarity matrices and the other evaluation metrics were obtained using Python 2.7.

Detailed information about our method, including the subjects used and processed, the processing specifications, the implementation of the patient selection software, and our result evaluation algorithm are available on the GitHub platform [15].

IV. Results

In this section, we describe how to interpret the similarity matrices obtained in the last step of our method and the results of applying well-known evaluation metrics. Note that ground-truth was not available and, thus, we could not comprehensively assess information on statistical region shape. Finally, while AD is known to simultaneously affect multiple brain regions, in this work, we have independently analyzed these regions.

Our method generated a similarity matrix for each region (*e.g.*, Fig. 3(a)). Theses matrices corresponds to the similarity of the features estimated on a subject-pair basis across the 500 subjects. These matrices can be described as: 1) the similarity value shows how similar two subjects are based on similarities in the covariance of their histograms; 2) the subjects were grouped based on their AD stage (*i.e.*, 100 subjects per stage as shown in Fig. 3(b)); and 3) higher covariances were displayed in red and lower covariances, in blue.

The confusion matrix and the evaluation metrics were not directly computed from the similarity matrix. Instead, additional processing was performed to better highlight changes across the AD stages. Stages temporally near the stage under investigation were grouped to make an expected positive group. Conversely, more temporally distant stages formed an expected negative group. The result dichotomized the stage data into expected positive and negative groups. We assumed that temporally neighboring stages should have higher correlation than more distant stages in the disease progression. Table II shows how stages were grouped to perform binary comparisons.

Once the positive and negative groups were identified, the confusion matrices were generated using Algorithm 1 to analyze how accurate the "prediction" of AD stages was, based on the shape of the regions. This algorithm was divided into two parts: 1) *Prediction*: The prediction is positive if the mean covariance of positive group is greater than or equal to the mean covariance of the negative subjects. 2) *Confusion matrix*: In order to estimate FN, FP, TN, and TP, the prediction is compared to patient ground-truth classification. Importantly, this algorithm is performed on a per region and per stage basis, following the details provided in Fig. 3. In Fig. 4, the evaluation metric results are shown for each stage and region.

V. Discussion

Image processing has been frequently applied to AD diagnosis and/or prognosis. Many studies are described in the literature and numerous computational methods have been developed to aid the understanding of underlying brain changes. Generally, these methods perform distinct assessments in order to classify AD (or MCI). Some methods use demographic data, familiar history, and cognitive testing in addition to brain imaging.

In this work we focus on how the shapes of individual brain regions vary with AD progression through the five ADNI-defined stages. The ventricles, cortical and deep gray matter structures were studied. Performing an analysis across multiple disease stages is non-trivial due to subtle overlap between temporally adjacent stages (*i.e.*, eMCI and lMCI with respect to MCI). We showed that shape descriptors that describe brain

TABLE II
Grouping of AD stages into positive and negative groups.

Stage Assessed	Positive Group	Negative Group
CN	CN, eMCI	MCI, lMCI, AD
eMCI	CN, eMCI, MCI	lMCI, AD
MCI	eMCI, MCI, lMCI	CN, AD
lMCI	MCI, lMCI, AD	CN, eMCI
AD	lMCI, AD	CN, eMCI, MCI

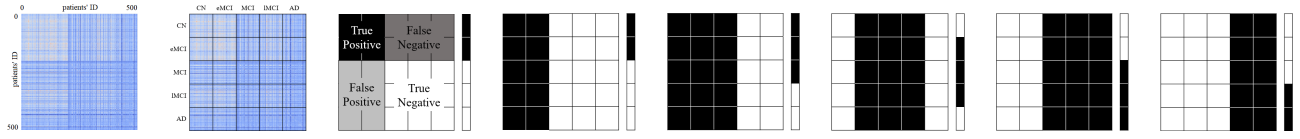

Fig. 3. Experiment overview: (a) outcome of the proposed method, where each row and column corresponds to one of the 500 subjects; (b) grouping of the subjects by stage (each 100×100 square denotes a distinct stage); (c) *e.g.*, template of the confusion values for CN stage; (d to h) division of subjects in two stages (positive [black] and negative [white]). The bar in (c-g) represents the ideal outcome. Shown are divisions for stages of interest (d) CN; (e) eMCI; (f) MCI; (g) lMCI; and (h) AD.

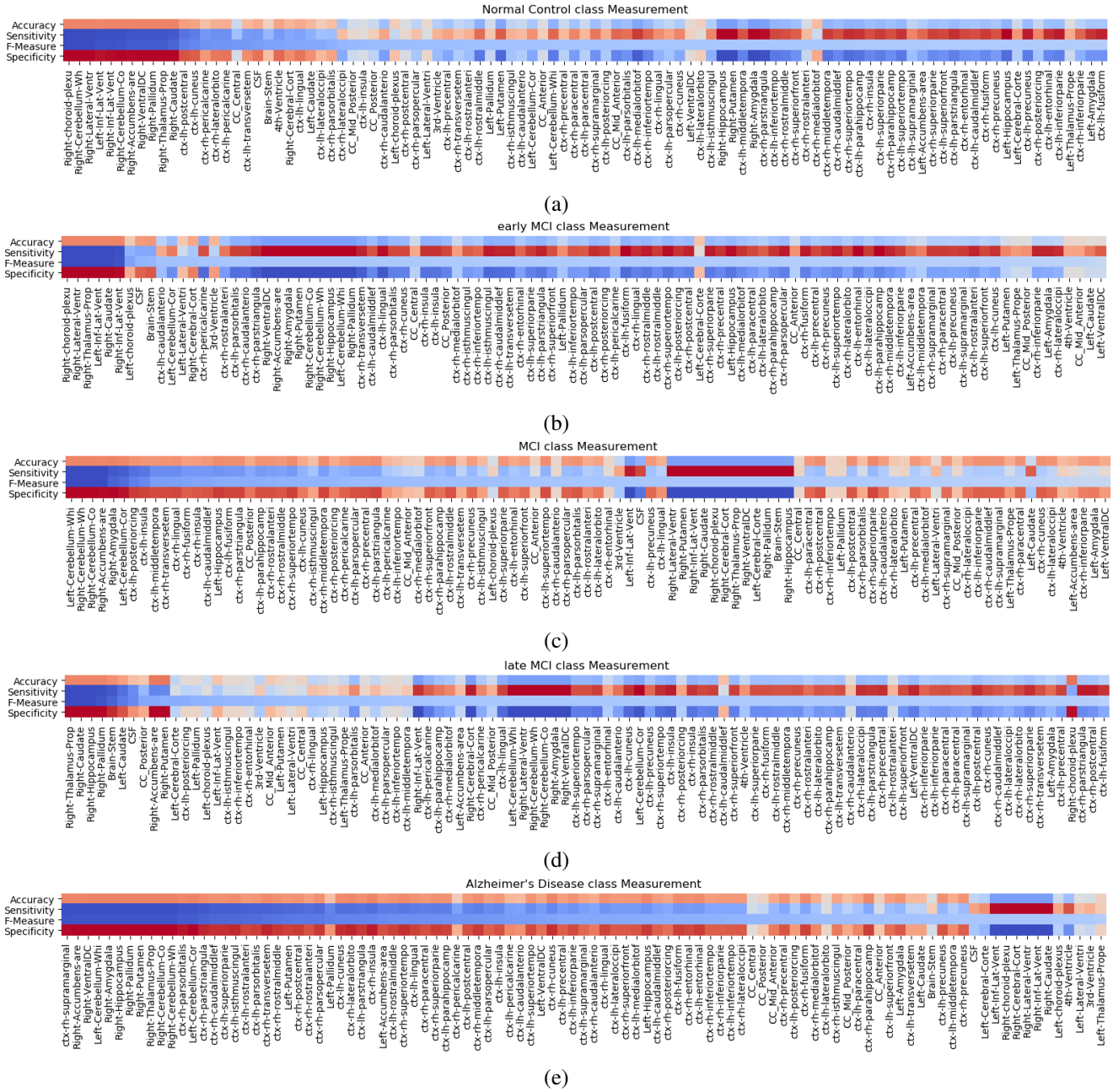

Fig. 4. Outcome of the assessment of each region by stage according to several metrics for: (a) CN, (b) eMCI, (c) MCI, (d) lMCI, and (e) AD analyses. Regions at each stage are sorted by F-score so that those with the highest association for change are to the right. The color bar ranges from blue (value $= 0$) to red (value $= 1$)

```
Data: vector gt[500], matrix simMatrix[500,500]
Result: integer TP, FP, TN, FN
initialization: pred[500] = null;
for i from 1 to 500 do
    if mean(simMatrix[i,Positive]) ≥
     mean(simMatrix[i,Negative]) then
        pred[i] ← Positive;
    else
        pred[i] ← Negative;
    end
end
for i from 1 to 500 do
    if pred[i] is Positive and gt[i] is Positive then
        TP ← TP + 1;
    else
        if pred[i] is Positive and gt[i] is Negative then
            FN ← FN + 1;
        else
            if pred[i] is Negative and gt[i] is Positive
             then
                FP ← FP + 1;
            else
                TN ← TN + 1;
            end
        end
    end
end
```

Algorithm 1: Confusion matrix values per region and stage. See Fig. 3(d to h) for positive and negative groups. See description in text.

regions, when invariant to scaling, are sensitive to identifying change (Fig. 4).

For further analysis, We grouped the gray matter results shown in Fig. 4 into 1) cortical regions and 2) deep regions. Cortical regions are assigned to every region label starting with "ctx", otherwise they were considered deep regions. The ventricles were also considered to be deep brain structures. After sorting by F-score, we obtained the first twenty regions at each stage (corresponding to highest F-score associated with $\approx 20\%$ of our regions). On a stage basis, we found that for gray matter: 1) CN: 75% were cortical and 25%, were deep regions; 2) eMCI: 55% were cortical and 45% were deep regions; 3) MCI: 55% were cortical and 45% were deep regions; 4) lMCI: 85% were cortical and 15% were deep regions; and 5) AD: 20% were cortical and 80% were deep regions. These interesting findings suggest a balance of regional change and cortical regions early in disease to deep structures by lMCI and more deep changes in the final AD stage of the disease. This suggests that examining cortical regions may lead to a better prediction in early stages (*e.g.*, CN $\rightarrow$ eMCI). Conversely, in later stage of the disease (*i.e.*, AD), examining the deep structures maybe more more predictive.

There are two significant limitations in our study: First, only cross-sectional data were used. Longitudinal data is available in the ADNI and other data sets and would potentially provide statistically more powerful results.

Second, Freesurfer segmentation separates white matter by hemisphere, rather than by lobe or tract. As a result the white matter regions were essentially global brain measures. Attempting to compute geometric words for large hemispheric white matter regions failed due to insufficient computer memory (results not shown). However, the process described in III.C successfully concluded when performing it on fewer subjects ($N = 25$). For reference, white matter corresponds to $\approx 40\%$ of the brain volume.

VI. Summary and Conclusion

In this work we presented a shape analysis method for selecting distinct brain regions related to AD progression. Our method is composed of four major steps:

1) *Data Acquisition and Selection*, which consists of obtaining T1-weighted MR volumetric T1w scans of 500 subjects (100 for each of five AD stages), after selecting the "best" scan per subject;
2) *Brain Segmentation and Mesh Conversion*, which consists of the brain segmentation using Freesurfer, and the conversion of each brain region onto a single mesh;
3) *Feature Extraction and Clustering*, which derives the 3D shape features from the meshes, and clusters these features into geometric words;
4) *Similarity Measurement*, where the covariance among different stages is measured.

The SIHKS provided 3D shape analysis for each brain region. We assumed that, regardless of region size, the shape played a key role in understanding AD progression. Indeed, our results show that shape features are potentially important for understanding AD progression.

We used the covariance between different stages to assess distinct regions. Some regions were found to predict specific AD stages. Ideally, regions which change more between stages of AD should present higher covariance. In contrast, lower covariance values should be obtained when comparing subjects from distinct stages.

In future studies, we intend to focus on incorporating the brain regions that provide the best discrimination between AD stages into an image retrieval technique, in order to accurately predict AD stages. Additionally, 3D shape features can also be adapted to machine learning approaches. Moreover, different brain regions are simultaneously affected in specific stages. Thus, a multi-region analysis could be a promising extension to single-region analysis.

Acknowledgment

Data collection and sharing for this project was funded by the ADNI (National Institutes of Health Grant U01 AG024904) and DOD ADNI (Department of Defense award number W81XWH-12-2-0012). ADNI is funded by the National Institute on Aging, the National Institute of Biomedical Imaging and Bioengineering, and through generous contributions from a number of other sponsors and foundations. The

authors thank Coordenação de Aperfeiçoamento de Pessoal de Nível Superior (CAPES, Brazil), the Canada Foundation for Innovation (CFI), and the Canadian Institutes for Health Research (CIHR) for research support. Special thanks is extended to the University of Campinas (UNICAMP) and University of Calgary.

REFERENCES

[1] C. A. Raji, O. L. Lopez, L. H. Kuller, O. T. Carmichael, and J. T. Becker, "Age, alzheimer disease, and brain structure," *Neurology*, vol. 73, no. 22, pp. 1899–1905, Oct. 2009. [Online]. Available: https://doi.org/10.1212/wnl.0b013e3181c3f293

[2] Y. Liu, B. Li, D. Elliman, P. S. Morgan, and D. Auer, "Automatic segmentation of putamen from brain mri," in *Advances in Neural Networks - ISNN 2006*, J. Wang, Z. Yi, J. M. Zurada, B.-L. Lu, and H. Yin, Eds. Berlin, Heidelberg: Springer Berlin Heidelberg, 2006, pp. 606–613.

[3] Chen Jia-lin, He Hua-can, and Liu Cheng-xia, "Feature extraction of brain ct image based on target shape," in *2009 Chinese Control and Decision Conference*, 2009, pp. 3553–3556.

[4] P. Zhu, S. P. Awate, S. Gerber, and R. Whitaker, "Fast shape-based nearest-neighbor search for brain mris using hierarchical feature matching," in *Medical Image Computing and Computer-Assisted Intervention – MICCAI 2011*, G. Fichtinger, A. Martel, and T. Peters, Eds. Berlin, Heidelberg: Springer Berlin Heidelberg, 2011, pp. 484–491.

[5] S. Lazebnik, C. Schmid, and J. Ponce, "Beyond bags of features: Spatial pyramid matching for recognizing natural scene categories," in *2006 IEEE Computer Society Conference on Computer Vision and Pattern Recognition (CVPR'06)*, vol. 2, 2006, pp. 2169–2178.

[6] S. Ghanavati, J. Li, T. Liu, P. S. Babyn, W. Doda, and G. Lampropoulos, "Automatic brain tumor detection in magnetic resonance images," in *2012 9th IEEE International Symposium on Biomedical Imaging (ISBI)*, 2012, pp. 574–577.

[7] A. Chaddad, C. Desrosiers, and T. Niazi, "Deep radiomic analysis of mri related to alzheimer's disease," *IEEE Access*, vol. 6, pp. 58 213–58 221, 2018.

[8] D. S. Marcus, T. H. Wang, J. Parker, J. G. Csernansky, J. C. Morris, and R. L. Buckner, "Open access series of imaging studies (OASIS): Cross-sectional MRI data in young, middle aged, nondemented, and demented older adults," *Journal of Cognitive Neuroscience*, vol. 19, no. 9, pp. 1498–1507, Sep. 2007. [Online]. Available: https://doi.org/10.1162/jocn.2007.19.9.1498

[9] B. Fischl, D. H. Salat, E. Busa, M. Albert, M. Dieterich, C. Haselgrove, A. van der Kouwe, R. Killiany, D. Kennedy, S. Klaveness, A. Montillo, N. Makris, B. Rosen, and A. M. Dale, "Whole brain segmentation: Automated labeling of neuroanatomical structures in the human brain," *Neuron*, vol. 33, no. 3, pp. 341–355, 2002. [Online]. Available: http://www.sciencedirect.com/science/article/pii/S089662730200569X

[10] P. Rajendran and M. Madheswaran, "An improved brain image classification technique with mining and shape prior segmentation procedure," *J. Med. Syst.*, vol. 36, no. 2, p. 747–764, Apr. 2012. [Online]. Available: https://doi.org/10.1007/s10916-010-9542-8

[11] S. Bu, Z. Liu, J. Han, J. Wu, and R. Ji, "Learning high-level feature by deep belief networks for 3-d model retrieval and recognition," *IEEE Transactions on Multimedia*, vol. 16, no. 8, pp. 2154–2167, 2014.

[12] J. Sun, M. Ovsjanikov, and L. Guibas, "A concise and provably informative multi-scale signature based on heat diffusion," in *Proceedings of the Symposium on Geometry Processing*, ser. SGP '09. Goslar, DEU: Eurographics Association, 2009, p. 1383–1392.

[13] M. M. Bronstein and I. Kokkinos, "Scale-invariant heat kernel signatures for non-rigid shape recognition," in *2010 IEEE Computer Society Conference on Computer Vision and Pattern Recognition*, 2010, pp. 1704–1711.

[14] Z. He, S. Bao, and A. Chung, "3D deep affine-invariant shape learning for brain mr image segmentation," in *Deep Learning in Medical Image Analysis and Multimodal Learning for Clinical Decision Support*, D. Stoyanov, Z. Taylor, G. Carneiro, T. Syeda-Mahmood, A. Martel, L. Maier-Hein, J. M. R. Tavares, A. Bradley, J. P. Papa, V. Belagiannis, J. C. Nascimento, Z. Lu, S. Conjeti, M. Moradi, H. Greenspan, and A. Madabhushi, Eds. Cham: Springer International Publishing, 2018, pp. 56–64.

[15] K. T. N. Duarte, "Alzheimers disease analysis," https://github.com/KaueTND/Alzheimers_Disease_analysis/, 2020.

[16] A. Klein and J. Tourville, "101 labeled brain images and a consistent human cortical labeling protocol," *Frontiers in Neuroscience*, vol. 6(171), p. 12, 2012. [Online]. Available: https://www.frontiersin.org/article/10.3389/fnins.2012.00171

[17] W. E. Lorensen and H. E. Cline, "Marching cubes: A high resolution 3D surface construction algorithm," *SIGGRAPH Comput. Graph.*, vol. 21, no. 4, pp. 163–169, Aug. 1987. [Online]. Available: https://doi.org/10.1145/37402.37422

[18] J. Sun, M. Ovsjanikov, and L. Guibas, "A concise and provably informative multi-scale signature based on heat diffusion," in *Proceedings of the Symposium on Geometry Processing*, ser. SGP '09. Goslar, DEU: Eurographics Association, 2009, p. 1383–1392.